Electronics and Electrical Engineering

http://www.aimspress.com/journal/ElectrEng

AIMS Electronics and Electrical Engineering, 7(4): 354–379.
DOI: 10.3934/electreng.2023019
Received: 26 June 2023
Revised: 01 October 2023
Accepted: 12 October 2023
Published: 25 October 2023

Research article

Sliding mode control rotor flux MRAS based speed sensorless induction motor traction drive control for electric vehicles

Saqib J Rind[1,*], Saba Javed[2], Yawar Rehman[2] and Mohsin Jamil[3]

[1] Department of Automotive & Marine Engineering, NED University of Engineering & Technology, University Road, Karachi, Pakistan
[2] Department of Electronics Engineering, NED University of Engineering & Technology, University Road, Karachi, Pakistan
[3] Department of Electrical & Computer Engineering, Faculty of Engineering and Applied Science, Memorial University of Newfoundland, 240 Prince Phillip Drive, St. John's, NL A1B 3X5, Canada

* **Correspondence:** Email: sjrind@neduet.edu.pk; Tel: +92-21-99261261-68.

Abstract: Climate change has highlighted a need to transition to more sustainable forms of transportation. Electric vehicles (EVs) and hybrid electric vehicles (HEVs) offer a promising alternative to conventional gasoline powered vehicles. However, advancements in power electronics and advanced control systems have made the implementation of high performance traction drives for EVs and HEVs easy. In this paper, a novel sliding mode control model reference adaptive system (SMC-MRAS) speed estimator in traction drive control application is presented. However, due to the unpredictable operational uncertainties of the machine parameters and unmodelled non-linear dynamics, the proportional-integral (PI)-MRAS may not produce a satisfactory performance. The Proposed estimator eliminates the PI controller employed in the conventional MRAS. This method utilizes two loops and generates two different error signals from the rotor flux and motor torques. The stability and dynamics of the SMC law are obtained through the Lyapunov theory. The potential of the proposed SMC-MRAS methodology is simulated and experimentally validated for an electric vehicle application. Matlab-Simulink environment is developed and proposed scheme is employed on indirect vector control method. However, for the experimental validation, the dSPACE 4011 R & D controller board was utilized. Furthermore, the SMC-MRAS performance is differentiated with PI-MRAS for speed regulation performance, tracking and estimation error, as well as the fast minimization of the error signal. The results of the proposed scheme illustrate the enhanced speed estimation, load disturbance rejection ability and fast error dynamics.

Keywords: electric vehicles; electric drives; induction motor control; MRAS; sensorless motor control; sliding mode control; traction drive

1. Introduction

The rapid reduction of fossil fuel resources, the continuous decline in air quality, hazardous emissions, various legislations towards the minimization of such emissions in the environment and the production of greenhouse gases due to internal combustion engine based vehicles have highlighted the need to develop an emission-free, healthy, environmental alternative energy vehicle [1–3]. The automotive industry largely contributes to the production of such harmful exhaust emissions in the environment, specifically in urban areas. Furthermore, the continuous consumption of fossil fuel resources may result in the reduction of non-renewable sources for other applications [1]. In the past two decades, automotive manufacturers have made substantial investments in cutting-edge technologies to mitigate environmental damage by meeting regulatory requirements. The research and development work in these technologies are primarily concentrated on enhancing the efficiency of internal combustion engines. This involves implementing innovations such as direct fuel injection, engine downsizing coupled with gearbox optimization, engine cylinder deactivation, and start-stop functionality. To further mitigate harmful emissions, it has become imperative to transition to an electrified propulsion system, which is characterized by an increased reliance on electrical energy for vehicle traction. Additionally, an electrified transportation system provides an appropriate solution to conserve fossil fuels and reduce air pollution for a clean environment [4]. In the case of hybrid electric vehicles (HEVs), depending on the degree of electrification or hybridization, the combination of conventional engine alongside an electric motor operation provides a wide range of advantages, such as a decrease in fuel consumption and emissions, and improved vehicle drivetrain operation. Extensive research and development activities have been conducting for the last couple of decades in order to penetrate the alternative energy vehicles into automotive industry [2].

Moreover, efficient operational optimization for the electric vehicle (EV) powertrain along with an appropriate mechanism for the enhanced performance of electric drive control contribute a significant step in the present research and development of a pure electrical transport system [5]. To ensure optimality, it is important to consider a systematic powertrain design and control approach, alongside an energy management strategy to produce the overall efficient electric propulsion system. However, in the case of an HEV, this powertain design and control approach is a bit complex, where the components of the conventional and pure EV are integrated into the same system. In addition, the continuous advancement in battery technology, power electronic devices and high performance electric machines contribute towards the production of highly energy-efficient electric propulsion system [6].

An electric motor control is considered a basic and necessary unit of EVs and HEVs [7]. The desired operating performance from the traction motor along with an appropriate compactness of the powertrain, minimum energy losses and a relatively high efficiency have an enormous impact in the establishment of electrified transport industry [1, 7]. Key considerations in EVs and HEVs electric propulsion include a high level of reliability and maintenance free powertrain operation. In addition, other key requirements include optimal energy management, optimal design of electric motor, suitable selection of drive train and control strategies [5]. Several electric motors have been studied for the establishment and growth of EV technology. There are several types of traction motors have been adopted by different EV manufacturers for electric propulsion [3]. In the past, direct current (DC) motors have been utilized by different EV manufacturers due to its simple and matured speed control mechanism. However, DC motors do not offer maintenance free operation and are not appropriate for

the applications where a high level of operational performance is required, as is the case for EVs and HEVs [5]. In contrast, AC motors, such as induction and synchronous machines, not only provide the maintenance free operation, but are also suitable for high performance, energy efficient, electric drive applications [3]. However, an induction motor (IM) is a widely accepted and remarkable candidate in EVs and HEVs due to several key characteristics such as ruggedness, reliability in operation, decreased cost, minimum required maintenance, aggressive environment operating suitability and improved transient performance [1, 3].

An electric motor drive is a part and parcel of various types of EVs & HEVs. Control of the electric motor is critical in EV technology as it determines the performance, efficiency, and range of the vehicle [5]. The advancement in electric machines used for electric vehicle technology and drive systems should be integrated with state-of-the-art fields and innovations. Over the past few years, several emerging technologies have been introduced such as the use of artificial intelligence technology, wireless charging infrastructure and system component integration [3]. Electric motors are the primary power source in EV, and its speed, torque, and output power must be precisely controlled to optimize the vehicle's operation. This control is achieved through advanced power electronics and control systems, which manage the electricity direction between the battery and motor in order to regulate the motor's output to meet the driver's demands [3]. A traction drive requires fast dynamic performance, which became possible after the technological improvements in power electronics, advanced data processing and implementation of artificial intelligence in order to enhance the system control and mechanical robustness [1, 7]. Advanced motor control techniques require accurate rotor position and speed information during control operation. However, the implementation of a mechanical speed encoder reduces the overall motor control performance due to signal distortion of the controllers and susceptibility of the electromagnetic interference [8,9]. Moreover, this increases the electric drive cost, reduces the mechanical robustness and injects the electrical noises in the computation process [8].

However, the requirement of a compact electric propulsion system appreciates the removal of a speed sensor or tachometer in the electric drive. Thus, the implementation of the conventional speed encoder on the motor shaft is not preferred due to operational reliability and physical constraints. The speed sensorless method offers several advantages, provided that an appropriate speed estimation algorithm is used [8]. Such schemes minimize the cost of transducers and hardware complexity and provide the compactness in the traction drive. Furthermore, these strategies offer higher electrical noise immunity, overall system reliability and mechanical robustness and are suitable for the hostile environment operation [8]. The implementation of the speed sensorless scheme in the EV drive train not only provides a fault tolerance feature in the system but also improves the operational robustness [3]. Motor operation control without using feedback sensor has become a huge source of attention since it provides an improved performance and simple implementation due to digital and analog signal processing schemes. This sensorless electric drive operation is preferred particularly, for the motor directly connected to the wheel architecture of the EV, where the bulky drive shaft mechanism and gearings are removed by direct connecting the motor in the wheel rim where torque and speed variations are required [1, 5].

There are two main methods for motor speed estimation: methods based on machine anisotropies or spectral analysis and methods based on machine mathematical models [3]. However, in the last couple of decades, various motor speed estimation methods have been suggested [9–16]. The model reference adaptive system (MRAS) is a widely used machine model-based adaptive control method

that requires machine operating voltages and currents to estimate the speed. This method offers simple implementation, operational effectiveness and minimal computational efforts in the design process [15]. Due to different error signals between the reference and the adjustable model, other MRAS variants include rotor flux, stator currents, reactive power and back electro motive force (EMF) [12]. Moreover, other techniques include the sliding mode scheme, the extended Kalman filter, X-MRAS, torque-MRAS and artificial intelligence incorporated schemes such as fuzzy logic, neural networks and fuzzy-neuro observers [10, 15].

Many machine-model schemes work on the estimation of stator and rotor fluxes. Flux determination through the voltage model is more common in such schemes. However, the calculation of pure integration associated in the voltage model exhibits two problems: dc saturation and offset and dc drift which is due to the initial condition problem in the integration [8]. Different strategies have been suggested to either eliminate or minimize the integrator problem in the voltage model. The most adopted approach is the utilization of low pass filter rather than the integrator; however, this approach suffers from an error in magnitude as well as in phase close to the corner frequency of the filter. However, the application and limitation of such schemes depend on the accuracy of flux estimation [8, 9]. Therefore, the selection of a particular motor that offers suitable traction drive characteristics and is associated with a sensorless control scheme largely contributes to the development of high performance, reliable and cost-effective EV / HEV traction drive train. In addition, these sensorless schemes are more dependent on the machine parameters, which are not constant during the operation; the continuous parameter estimation is required for an accurate speed estimation in the control [3]. However, the operating conditions of the EV motor drive is complicated; therefore, the sensoless control mechanism should be capable of handling torque variations and disturbances. Most of the sensorless schemes have been focused on steady state performance, while the dynamic performance of such techniques need to be investigated further. The estimation performance of methods based on machine anisotropies, such as signal injection at low speed condition, has an additional loss and filter, which is used to further overcome the issue of deterioration of the position estimation accuracy [3]. Hence, the adoption of any scheme should make sure an adequate operation of the motor drive, which is capable of providing an acceptable performance of the motor in all four quadrants for the application of EVs and HEVs [17].

Several studies have been conducted to manage the operational performance of an electric drive. However, an inaccurate estimation at very low speeds and poor performance during the applied load variations are still serious issues of such speed estimation schemes and have not been resolved completely yet [8]. Almost all associated MRAS variants have been used with a fixed gain PI controller in an adaptation mechanism. However, the continuous motor parameters variation, inverter non-linearity, and controller signal distortions may not provide a satisfactory performance of the IM drive with fixed-gain PI controller [18]. As a result, investigating an additional form of the adaptation mechanism becomes crucial for reducing speed tuning signals or error signals and achieving a precise speed estimation for smooth drive operation.

Nowadays, the sliding mode control (SMC) method is gaining the increased attention of researchers in speed sensorless control of machines [19–21]. Speed observers based on SMC have been introduced to estimate the parameters of induction machines. However, diverse SM strategies have emerged as potential solutions for governing the operation of induction machine drives. The SMC approach is an effective and robust control technique due to its ability to handle disturbances and model inaccuracies,

making it well-suited for controlling nonlinear IM drives. This approach involves formulating a switching control strategy. To achieve this, the Lyapunov theory is employed to ensure that the state trajectory converges toward the sliding surface, while adjusting the control gain to ensure a negative definite derivative of the Lyapunov function [18]. In general, along with its uncomplicated structure, the SMC approach demonstrates robustness. These key characteristics establish SMC as the predominant model-based method for speed sensorless control in various applications [18, 19]. There is an extensive review of the SMC observer in sensorless control of electric drives [22]. In this paper, a classical SMC strategy has been modified to address the estimation problem and a new SMC-MRAS has been developed. Therefore, the suggested scheme removes the constant gain PI controller to the SMC and uses two loops (i.e., inner and outer) with different error signals for the improved speed estimation under load disturbance conditions.

This paper is comprised of eight sections. In Sections 2 & 3, vehicle dynamics for the required tractive force for electric propulsion and IM non-linear ($d - q$ model) for vector control operation are presented. Sections 4 & 5 explain the PI-MRAS modelling and the suggested sliding mode MRAS scheme. Different cases of simulation and experimental results are discussed and performance of the proposed SMC-MRAS are investigated in Sections 6 & 7, respectively. Section 8 presents the conclusion of the paper.

2. Vehicle dynamics

The knowledge of vehicle dynamics is important to calculate the total tractive effort required for a vehicle movement. This propelling force between the driving wheels and road surface is responsible for vehicle acceleration. A vehicle moving in the uphill direction will have different forces acting on the vehicle body to retard its motion, as shown in Figure 1. The vehicle rate of change of velocity can be expressed as follows [23]:

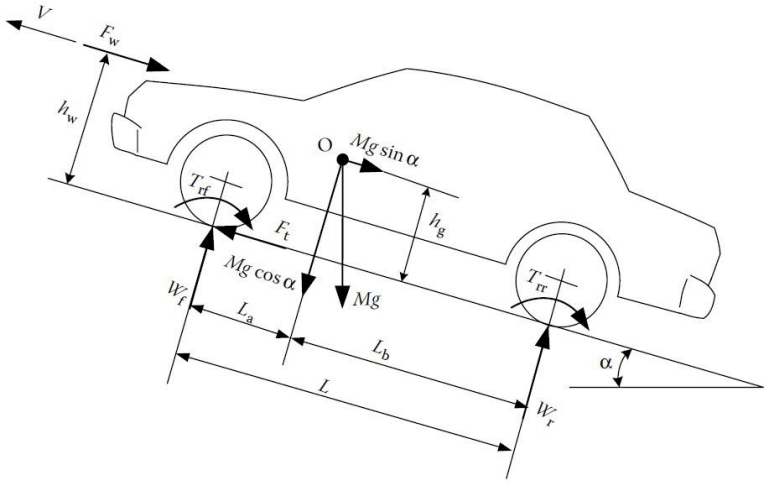

Figure 1. Different acting forces on vehicle [23].

$$\frac{dV}{dt} = \frac{\sum F_t - \sum F_{tr}}{\delta M_v}, \tag{1}$$

where $\sum F_t$ is the total tractive effort and $\sum F_{tr}$ is the total resistive forces against the vehicle movement, (M_v,V) represents the vehicle mass and velocity, respectively, and δ is the mass factor. The Vehicle longitudinal movement can be expressed as follows:

$$M_v \frac{dV}{dt} = (F_{tf} + F_{tr}) - (F_{rf} + F_{rr} + F_w + F_g). \tag{2}$$

The total operational tractive forces of the vehicle from both the front F_{tf} and back tires F_{tr} are responsible for vehicle acceleration, provided that all the resisting forces on the vehicle, such as front and back tires rolling resistance, F_{rf} & F_{rr} respectively, aerodynamic drag F_w, and climbing resistance F_g, must be lower than the applied tractive force.

Rolling resistance (sometimes called rolling drag) is the resisting force when the body rolls on the surface, as caused by non-elastic effects, and can be expressed as follows:

$$F_r = P f_r \cos\alpha. \tag{3}$$

The rolling resistance coefficient f_r depends on tire inflation pressure, tire temperature and condition of the vehicle operating road. However, P is the normal force and α is the associated angle from the road surface. By means of low resistance tires or a lower value for f_r, the fuel consumption of the vehicle can be saved. Reducing the rolling resistance can improve the vehicle fuel efficiency and reduce the energy consumption, which is an important consideration in vehicle design and operation.

Aerodynamic drag or air resistance force that opposes the vehicle's motion through the air and depends on the air density ρ, vehicle body shape & its frontal area A_f, velocity V, and wind speed V_w, and mathematically can be written as follows [23]:

$$F_w = \frac{1}{2}\rho A_f C_D (V - V_w)^2, \tag{4}$$

where C_D is drag coefficient and V_w is speed of the air with respect to the vehicle motion. The vehicle fuel efficiency can be improved through the reduced aerodynamic drag, particularly at higher speeds, where it significantly contributes to the total energy consumption.

Finally, the grading resistance in a vehicle is the force that opposes the movement as the vehicle moves up or down a hill or incline. It is caused by the vehicle's weight and angle of the slope, and is influenced by factors such as the grade of the slope, the vehicle's speed and acceleration, and the characteristics of the surface such as friction and surface roughness. It can be written as follows:

$$F_g = M_v g \sin\alpha. \tag{5}$$

To reduce the grading resistance, vehicles may be designed with a lower center of gravity, optimized weight distribution, and specialized transmissions or gearings that can provide more torque and power at lower speeds.

The total operational tractive force can be represented as follows:

$$F_t = F_{tf} + F_{tr} \tag{6}$$

Similarly, the maximum propulsion force required for a rear and front wheel drive system is [23].

$$F_{t_{\max}} = \frac{\mu M_v g \cos\alpha [L_a - f_r(h_g - r_d)]}{L - \mu h_g} \tag{7}$$

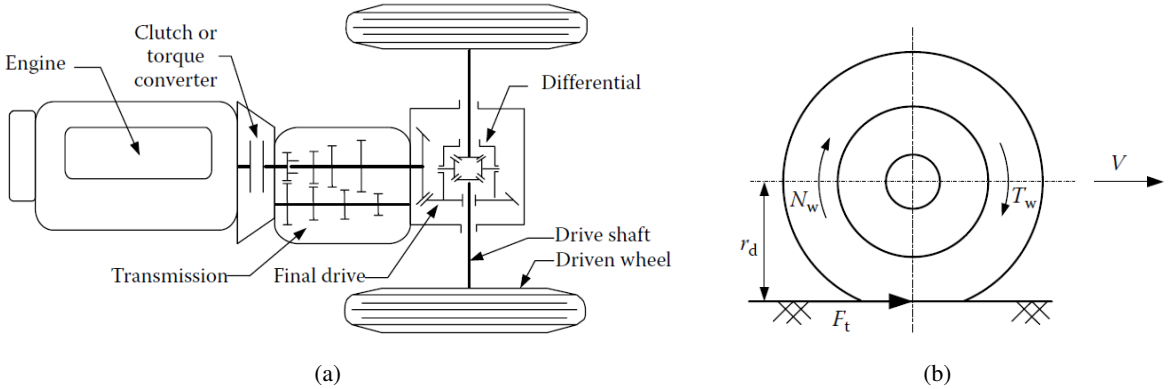

Figure 2. Vehicle power-train [23] 2(a) automobile power train illustration, 2(b) torque on driven wheel

$$F_{t_{\max}} = \frac{\mu M_v g \cos\alpha[L_b + f_r(h_g - r_d)]}{L + \mu h_g} \tag{8}$$

respectively, where μ is the road adhesion coefficient and r_d is the tire effective radius.

Figure 2(a) displays an automobile power train. The torque on the wheels can be written as follows:

$$T_w = i_g i_o \eta_t T_p, \tag{9}$$

where i_g & i_o represent the gear ratio of the transmission and the final drive, respectively. Additionally, η_t & T_p are the driveline efficiency and the power plant output torque, respectively. The tractive effort, as shown in Figure 2(b), can be written as follows:

$$F_t = \frac{T_w}{r_d}. \tag{10}$$

Substituting Eq (9) into Eq (10) yields the following:

$$F_t = \frac{T_p i_g i_o \eta_t}{r_d}. \tag{11}$$

The driven wheel rotating speed (rpm) is expressed as follows:

$$N_w = \frac{\omega_r^*}{i_g i_o}, \tag{12}$$

where ω_r^* is the transmission speed (rpm), which represents the traction motor speed. The vehicle translational speed can be written as follows:

$$V_{ref} = \frac{\pi N_w r_d}{30}, (m/s). \tag{13}$$

Substituting Eq (12) into Eq (13) results in the following:

$$V_{ref} = \frac{\pi \omega_r^* r_d}{30 i_g i_o}, (m/s). \tag{14}$$

Finally, the reference speed and load torque on the motor side after the electric vehicle mechanical transmission and gearbox can be expressed as follows: [23]:

$$\omega_r^* = \frac{30 i_g i_o V_{ref}}{\pi r_d} \tag{15}$$

$$T_l = \frac{r_d}{i_g i_o \eta_t} \left(F_r + F_w + M_v g \sin\alpha\right). \tag{16}$$

3. Induction motor model

The induction motor d-q model is an important tool for analyzing and designing electric motor control systems. This model provides a detailed understanding of the motor's behavior under different conditions in order to optimize the motor's performance, efficiency, and reliability. When the motor is operated using a fixed and balanced sinusoidal voltage supply, an IM circuit is utilized to calculate the important motor operational parameters [8]. However, the machine equivalent circuit model is not suitable for an operation analysis, specifically when it is operated by a non-sinusoidal voltage supply such as converter fed machines. In a variable frequency drive (VFD) operation, both steady state and transient conditions are to be analyzed to evaluate the performance of an IM.

This non-linear mathematical model of an IM is obtained by using the two axis direct-quadrature $(d-q)$ theory. In this model, all three phase machine parameters such as currents, voltages and fluxes are represented in their equivalent two phase stationary quantities and provide a simplicity in the design and analysis processes. Both Clarke and Park transformations are used to convert the three phase variables into their two phase stationary quantities and then their two phase rotating, respectively [8, 24]. This transformation process not only provides a simplification in the three phase machine analysis, but also provides the convenience to control the three phase inverter. A high performance ac drive method, such as flux oriented control, requires a good understanding of the machine two phase model for implementation.

This paper uses Krause's non-linear IM model. By means of flux linkages, the IM dynamic model can be written in a synchronous frame as follows [24]:

$$\frac{d\psi_{sQ}}{dt} = \omega_b \left[v_{sQ} - \frac{\omega_e}{\omega_b}\psi_{sD} - \frac{R_s}{X_{ls}}\left(\psi_{sQ} - \psi_{mQ}\right)\right] \tag{17}$$

$$\frac{d\psi_{sD}}{dt} = \omega_b \left[v_{sD} + \frac{\omega_e}{\omega_b}\psi_{sQ} - \frac{R_s}{X_{ls}}\left(\psi_{sD} - \psi_{mD}\right)\right] \tag{18}$$

$$\frac{d\psi_{rQ}}{dt} = -\omega_b \left[\frac{(\omega_e - \omega_r)}{\omega_b}\psi_{rD} + \frac{R_r}{X_{lr}}\left(\psi_{rQ} - \psi_{mQ}\right)\right] \tag{19}$$

$$\frac{d\psi_{rD}}{dt} = -\omega_b \left[-\frac{(\omega_e - \omega_r)}{\omega_b}\psi_{rQ} + \frac{R_r}{X_{lr}}\left(\psi_{rD} - \psi_{mD}\right)\right], \tag{20}$$

where ψ_{sD}, ψ_{sQ}, ψ_{rD}, ψ_{rQ}, ψ_{mD},ψ_{mQ}, V_{sD} and V_{sQ} are stator and rotor flux linkages, magnetizing flux linkages and voltages in the D-Q frame, respectively, R_s, R_r, X_{ls} & X_{lr} are stator and rotor resistances, and leakage reactance, respectively, and ω_b, ω_e and ω_r the machine base frequency, synchronous and rotor speed, respectively.

From this model, the torque and speed can be written as follows [24]:

$$T_e = \frac{3}{2}\left(\frac{P}{2}\right)\frac{1}{\omega_b}\left(\psi_{sD}i_{sQ} - \psi_{sQ}i_{sD}\right) \tag{21}$$

$$\frac{d\omega_r}{dt} = \left(\frac{P}{2J}\right)(T_e - T_l)\,, \tag{22}$$

where J, P and T_l denote the viscous coefficient, machine poles and load torque, respectively.

4. Conventional rotor flux-MRAS observer

Among several motor speed estimation strategies, MRAS is a more common and well established scheme in sensorless IM drive control due to its simplicity, direct physical interpretation and operational effectiveness [24]. The MRAS contains a basic parallel structure, and is comprised of a reference model, an adaptive model and an adaptation mechanism. There are different types of rotor speed MRAS observers and are based on the error signal generated from the reference and adjustable models. The reference model is also known as the voltage model since the model depends on IM stator voltage equations. Additionally, the adaptive model is known as the current model since it includes IM stator currents. Unlike the reference model, an adaptive model is based on a set of equations that contain the parameter to be estimated, in this case, the rotor speed. Both the reference and adaptive models are used to generate the error or speed tuning signal. This error signal is continuously minimized through an appropriate mechanism, such as a PI-controller in conventional MRAS, in order to accurately estimate the desired parameter. In the case of rotor flux MRAS, both models are used to generate the reference (ψ_{rD}, ψ_{rQ}) and estimated $(\hat{\psi}_{rD}, \hat{\psi}_{rQ})$ values of rotor flux, as shown in Figure 3.

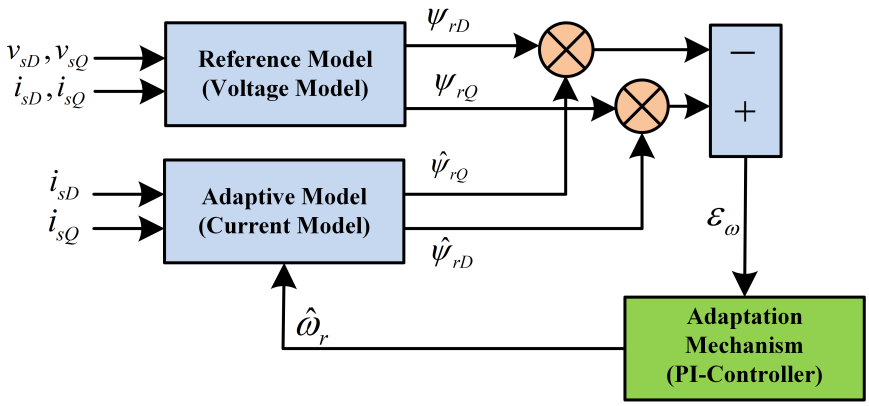

Figure 3. Rotor flux conventional PI-MRAS.

The stator voltage equation is expressed in stator reference frame as follows [24–26]:

$$v_s^s = R_s i_s^s + \sigma L_s p i_s^s + \frac{L_m}{L_r} p\psi_r^s \tag{23}$$

where the superscript s indicates the stator reference frame, p represents the derivative operator, L_m represents the mutual inductance, L_s represents the stator self inductance and L_r represents the rotor self inductance. The aforementioned Eq (23) can also be expressed in $d-q$ components of reference rotor fluxes:

$$\psi_{rD} = \frac{L_r}{L_m}\left[\int (v_{sD} - R_s i_{sD})dt - \sigma L_s i_{sD}\right] \tag{24}$$

$$\psi_{rQ} = \frac{L_r}{L_m}[\int (v_{sQ} - R_s i_{sQ})dt - \sigma L_s i_{sQ}], \tag{25}$$

where σ is an inductance leakage coefficient,

$$\sigma = 1 - \frac{L_m^2}{L_s L_r}.$$

The rotor voltage equations can be expressed in the same coordinates as [24–26]:

$$v_r^s = R_r i_r^s + \frac{d\psi_r^s}{dt} - j\omega_r \psi_r^s. \tag{26}$$

The aforementioned Eq (26) can be expressed in terms of estimated rotor fluxes as follows:

$$\frac{d\hat{\psi}_{rQ}}{dt} = -\frac{1}{T_r}\hat{\psi}_{rQ} + \hat{\omega}_r \hat{\psi}_{rD} + \frac{L_m}{T_r} i_{sQ} \tag{27}$$

$$\frac{d\hat{\psi}_{rD}}{dt} = -\frac{1}{T_r}\hat{\psi}_{rD} - \hat{\omega}_r \hat{\psi}_{rQ} + \frac{L_m}{T_r} i_{sD} \tag{28}$$

where $T_r = \frac{L_r}{R_r}$ is rotor time constant. It should be noted that the reference model is based on (24) & (25), whereas the adaptive model is based on (27) & (28). Finally, the error signal is computed in order to achieve the estimated speed as follows [24, 25, 27]:

$$\varepsilon_\omega = \psi_{rq}\hat{\psi}_{rd} - \psi_{rd}\hat{\psi}_{rq} \tag{29}$$

$$\hat{\omega}_r = (k_p + \frac{k_i}{p})\varepsilon_\omega. \tag{30}$$

In this case, the error signal is further passed through the fixed gain PI controller based adaptation mechanism so as to estimate the desired physical quantity and rotor speed. This PI controller continuously minimizes the error signal until this becomes zero and the estimated value approaches to the reference value [25]. Popov's Hyperstability theory is one of the most commonly employed approaches to design an appropriate adaptation mechanism. Additionally, the hyperstability theory can be used in order to design MRAS and provide detailed design steps [28].

5. Proposed sliding mode control MRAS

The proposed SMC-MRAS utilizes two different loops and generates two different error signals for an accurate rotor speed estimation. The first inner loop is used to determine the reference (ψ_{rD}, ψ_{rQ}) and estimated flux values $(\hat{\psi}_{rD}, \hat{\psi}_{rQ})$. In the proposed scheme, the associated rotor flux error signal passes through the SMC instead of the constant gain linear PI controller used in classical RF-MRAS. However, the outer loop uses the same sub models for reference and estimated rotor flux to take the difference between the reference and estimated electromagnetic torque T_e , $\hat{T}_e$ respectively [29]. Based on electromagnetic torques, this error signal improves the rotor speed estimation performance, specifically in the transient operating condition and the load disturbance condition. The Proposed SMC-MRAS block diagram is illustrated in Figure 4.

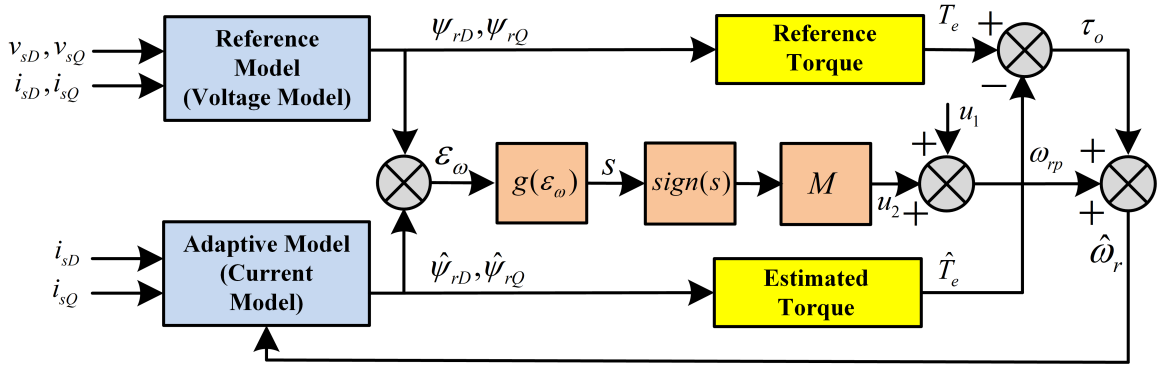

Figure 4. Proposed SMC-MRAS block diagram.

A non-linear adaptation mechanism of SMC-MRAS is obtained through the Lyapunov theory. The stability in the rotor speed estimation and quick error signal convergence towards the zero is achieved in the estimation process [18]. The error signal in Eq (29) is used to express the sliding surface s with an integral component as follows [18]:

$$s = \varepsilon_\omega + \int k\varepsilon_\omega dt, \qquad k > 0 \tag{31}$$

At $s = 0$, the error dynamics will force an exponentially decay to zero . The system approaches the sliding surface when

$$\dot{s} = \dot{\varepsilon}_\omega + k\varepsilon_\omega = 0. \tag{32}$$

Then, the error dynamics will be as follows:

$$\dot{\varepsilon}_\omega = -k\varepsilon_\omega. \tag{33}$$

The Lyapunov theory is used to represent the SMC law, and the following function is considered [30]:

$$v = \frac{1}{2}s^2. \tag{34}$$

As per Lyapunov's theory, if the derivative of the function defined in Eq (34) $\dot{v}$ is a negative definite, then the state trajectory will be driven and pulled towards the sliding surface s. Once the sliding surface is reached, the state will stay on it until it reaches the origin asymptotically [30].

The derivative of Eq (34) is as follows:

$$\dot{v} = s\dot{s} = s(\dot{\varepsilon}_\omega + k\varepsilon_\omega). \tag{35}$$

Differentiating the error signal in Eq (29) results in the following:

$$\dot{\varepsilon}_\omega = \dot{\psi}_{rQ}\hat{\psi}_{rD} + \psi_{rQ}\dot{\hat{\psi}}_{rD} - \dot{\psi}_{rD}\hat{\psi}_{rQ} - \psi_{rD}\dot{\hat{\psi}}_{rQ}. \tag{36}$$

Substituting flux components from (27) & (28) results in the following:

$$\dot{\varepsilon}_\omega = \dot{\psi}_{rQ}\hat{\psi}_{rD} - \dot{\psi}_{rD}\hat{\psi}_{rQ} + \frac{L_m}{T_r}i_{sD}\psi_{rQ} - \frac{1}{T_r}\hat{\psi}_{rD}\psi_{rQ} - \frac{L_m}{T_r}i_{sQ}\psi_{rD} + \frac{1}{T_r}\hat{\psi}_{rQ}\psi_{rD} - \hat{\omega}_r(\psi_{rQ}\hat{\psi}_{rQ} + \psi_{rD}\hat{\psi}_{rD}). \tag{37}$$

Consider the following:

$$B_1 = \dot{\psi}_{rQ}\hat{\psi}_{rD} - \dot{\psi}_{rD}\hat{\psi}_{rQ} + \frac{L_m}{T_r} i_{sD}\psi_{rQ} - \frac{1}{T_r}\hat{\psi}_{rD}\psi_{rQ} - \frac{L_m}{T_r} i_{sQ}\psi_{rD} + \frac{1}{T_r}\hat{\psi}_{rQ}\psi_{rD}. \tag{38}$$

$$B_2 = \psi_{rQ}\hat{\psi}_{rQ} + \psi_{rD}\hat{\psi}_{rD} \tag{39}$$

Equation (37) can be simplified as follows:

$$\dot{\varepsilon}_\omega = B_1 - \hat{\omega}_r B_2. \tag{40}$$

Now, Eq (32) will become the following:

$$\dot{s} = B_1 + k\varepsilon_\omega - \hat{\omega}_r B_2. \tag{41}$$

By substituting (40) into (35),

$$\dot{v} = s(B_1 + k\varepsilon_\omega - \hat{\omega}_r B_2). \tag{42}$$

The above equation is a negative definite, provided that

$$(B_1 + k\varepsilon_\omega - \hat{\omega}_r B_2)\begin{cases} < 0, & \text{for } s > 0 \\ = 0, & \text{for } s = 0 \\ > 0, & \text{for } s < 0. \end{cases} \tag{43}$$

if

$$\hat{\omega}_r = \frac{B_1 + k\varepsilon_\omega}{B_2} + (N)\, sign\,(s)\,, \qquad N > 0 \tag{44}$$

where the sign function is

$$sign(s) = \begin{cases} -1, & \text{for } s < 0 \\ +1, & \text{for } s > 0. \end{cases} \tag{45}$$

Here, Equation (44) explains the SMC switching law and can be expressed as follows:

$$\hat{\omega}_r = x_1 + x_2 \tag{46}$$

where x_1 and x_2 are the equivalent control and switching control, respectively. The state trajectory is kept on the sliding surface through control action x_1. However, x_2 depends on the sign of the switching surface and N is the hitting control gain, which makes Eq (35) a negative definite [30]. No particular design methodology is adopted to assign the value of N. The value of N is taken in such a way to make the manifold $s = 0$ in Eq (31) [30, 31]. However, the control law expressed in Eq (44) will make sure the existence of the switching surface s in Eq (31); and when the error function ε_ω reaches the sliding surface, the system dynamics will be controlled by Eq. (33), which is always stable [32].

Both x_1 and x_2 can be expressed as follows:

$$x_1 = \frac{B_1 + k\varepsilon_\omega}{B_2} \tag{47}$$

$$x_2 = (N)\, sign\,(s)\,, \qquad N > 0. \tag{48}$$

Lyapunov's direct method may be used to see if the derivative of the Lyapunov's function leads to asymptotic stability. In order to obtain this relation, the following assumptions should be formulated:

1. Assume that $k\varepsilon_\omega$ (the control error term) is small. This assumption is often made in the stability analysis to focus on the behavior near the equilibrium.
2. Assume that the switching law $\hat{\omega}_r = x_1 + x_2$ maintains the sliding surface, which implies that x_1 and x_2 are designed to achieve this stability.

Utilizing both aforementioned assumptions points, we can focus on the dominant terms B_1 and $-x_1B_2$. If $B_1 < 0$ (which implies that the control action is effective in driving the system towards the sliding surface) and if $x_1 > 0$ (which ensures that the equivalent control maintains stability), then the dominant terms will work to drive the derivative $\dot{V}$ towards negative values, indicating convergence towards the sliding surface. The Lyapunov direct method states that if $\dot{V}$ is a negative definite, then the system's trajectory will asymptotically converge to the sliding surface.

In the proposed observer, the speed component in Eq (46) can be written as a pre-processed speed component:

$$\omega_{rp} = x_1 + x_2 \tag{49}$$

Outer loop of the proposed scheme generates the electromagnetic error signal with the help of reference and estimated electromagnetic torques. The motor speed is expressed as follows:

$$T_e - T_l = J\frac{d\omega_r}{dt} + f\omega_r \tag{50}$$

If T_l and f are unknown, then Eq (50) is expressed as follows:

$$T_e - T = J\frac{d\omega_r}{dt}, \tag{51}$$

where $T = T_l + f\omega_r$.

The reference torque component is expressed as follows:

$$T_e = \frac{PL_m}{L_r}(i_{sQ}\psi_{rD} - i_{sD}\psi_{rQ}). \tag{52}$$

Similarly, the electromagnetic torque is derived from the estimated fluxes:

$$\hat{T}_e = \frac{PL_m}{L_r}(i_{sQ}\hat{\psi}_{rD} - i_{sD}\hat{\psi}_{rQ}). \tag{53}$$

Eq (50) describes the mechanical dynamics of the motor. It is observed that variations in the load results in changes in the motor speed, and this continues either until a steady state is reached or until the load torque on the motor becomes equal to the motor's torque.

The same concept applies to the estimated torque, where changes in the estimated torque result in changes in the motor's estimated speed, and this continues either until a steady state is achieved or until the estimated component of torque becomes equal to the motor's reference torque. The dynamics outlined in Eq (50) allow for the estimated torque and motor speed as follows:

$$\hat{T}_e - T_l = J\frac{d\hat{\omega}_r}{dt} + f\hat{\omega}_r. \tag{54}$$

By subtracting the Eq (54) from (50), the following equation is produced:

$$\tau_o = T_e - \hat{T}_e = J\frac{d(\omega_r - \hat{\omega}_r)}{dt} + f(\omega_r - \hat{\omega}_r) \tag{55}$$

Finally, the estimated speed can be expressed as follows:

$$\hat{\omega}_r = \omega_{rp} + \tau_o \tag{56}$$

Eq (55) states the aim of using this second torque loop in the proposed scheme. The variation in the estimated and reference torque will appear when the rate of change in estimated and the reference speed will appear in the dynamic mode of operation or under load disturbance condition. However, this second loop improves the motor speed estimation under different operating conditions, specifically in the load torque disturbance condition.

6. Simulation results & discussion

The MATLAB-Simulink platform was utilized for the performance evaluation of both PI-MRAS and the proposed SMC-MRAS. For this purpose, various simulation cases were made according to the vehicle operationl requirement. Different vehicle speed profiles and rated load torques with variation of operational conditions were used. The performance was evaluated through speed regulation, speed estimation, tracking errors and an error signal convergence to zero. The estimation error is defined as how much the estimated speed from the observer is deviated from the motor actual speed. However, the tracking error is the deviation of the estimated speed from the command speed.

Both observers are applied in an indirect vector control speed sensorless drive. The IM non-linear d-q model described in the synchronous frame is directly controlled with reference voltages so that the ideal inverter operation or pulse width modulation is considered in all simulation cases. Controller gains in the vector control method are similar for all simulation cases. However, the values for these gains and IM parameters and ratings can be found in Appendix Table 1 and Table 2, respectively. The implementation of the proposed SMC-MRAS sensorless IM drive control is shown in Figure 5.

The vehicle motion operation is maintained with two control. The first control is the motor speed, acceleration control, or driver's applied twisting force for the prolusion purpose. Another control is the vehicle brake operation, which is the applied load torque on the motor. During the whole operation of the vehicle, the motor speed and load torque parameters both change, such as uphill, downhill and un-smooth road conditions. However, the proposed speed observer should be capable of dealing with all operational situations. Different operating conditions are used for this simulation purpose in order to evaluate the estimator performance in the following section.

6.1. Estimator load disturbance rejection capability performance

The objective of this simulation is to evaluate and compare the load disturbance rejection performance of the suggested scheme with PI-MRAS. In this test, it is required that during the transient mode or when the load is acted, the proposed observer should be less deviated and should respond close to the real motor speed. The deterioration in the estimation speed should be as minimal as possible with respect to the actual motor speed. However, this simulation case is very important for the implementation of the speed observer in the EV traction drive. During the whole operation of the vehicle, the acting load is very uncertain and changes with operating conditions, such as an uphill mode of operation, downhill, aerodynamic effects, smooth and un-smooth road condition, etc.

For this purpose, the proposed and conventional observer performances are checked at 15 rad/sec motor speed with 60% rated load at $t = 3s$. The performance of the proposed observer algorithm

provides much lower values of both errors (estimation and tracking), along with the speed regulation performance. The error signal convergence to zero is quicker, which provides improved error dynamics and a transient response. For better performance understanding, a deviation in response between both estimators at $t = 3s$ is zoomed. In the proposed SMC-MRAS, the estimation error is reduced from 26.04% to 4.89%, and the tracking error is reduced from 52.78% to 33.33%. However, the value of speed tuning or error signal settling time is reduced from $t = 3.64s$ to $t = 3.159s$. Figures 6, 7 and 8 illustrate the key performance indicators in response to the observer for the load torque disturbance rejection capability.

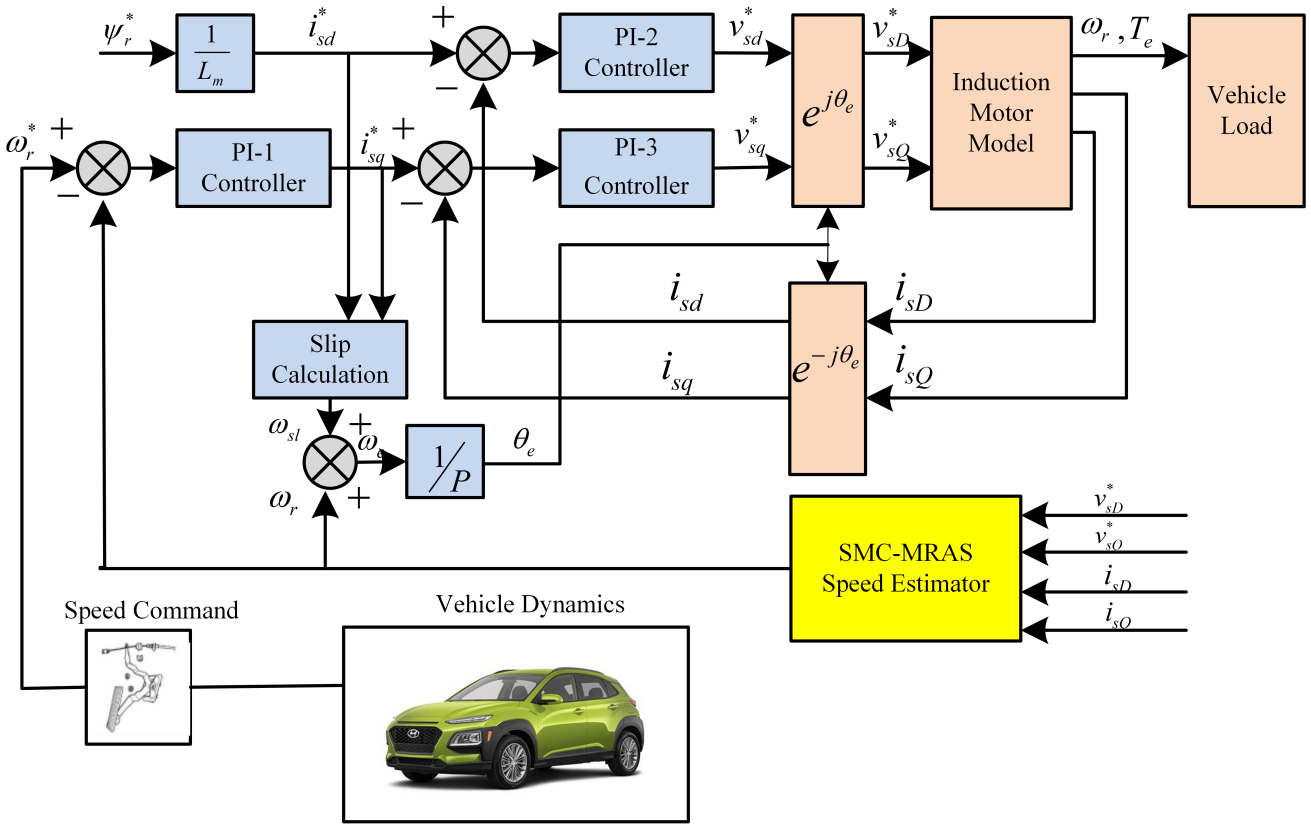

Figure 5. Proposed SMC-MRAS observer implementation on sensorless traction drive control.

6.2. *Quick acceleration performance*

The basic objective of this simulation is to evaluate the proposed observer performance in either a sudden motor speed change or in fast acceleration. This test is important either when the vehicle is operated in cruising mode of operation or when the high electromagnetic torque and acceleration are required in the start. In this control mechanism, the actual motor speed should approach the reference speed. However, the proposed observer speed estimation should be close to the real motor speed.

In this evaluation, a quick speed change from 0 to 15 rad/sec with 25% rated load is applied at $t = 0.5s$. The recommended speed observer provides fast error dynamics with a decreased speed estimation error as compared to PI-MRAS. However, in the proposed observer mechanism, the motor

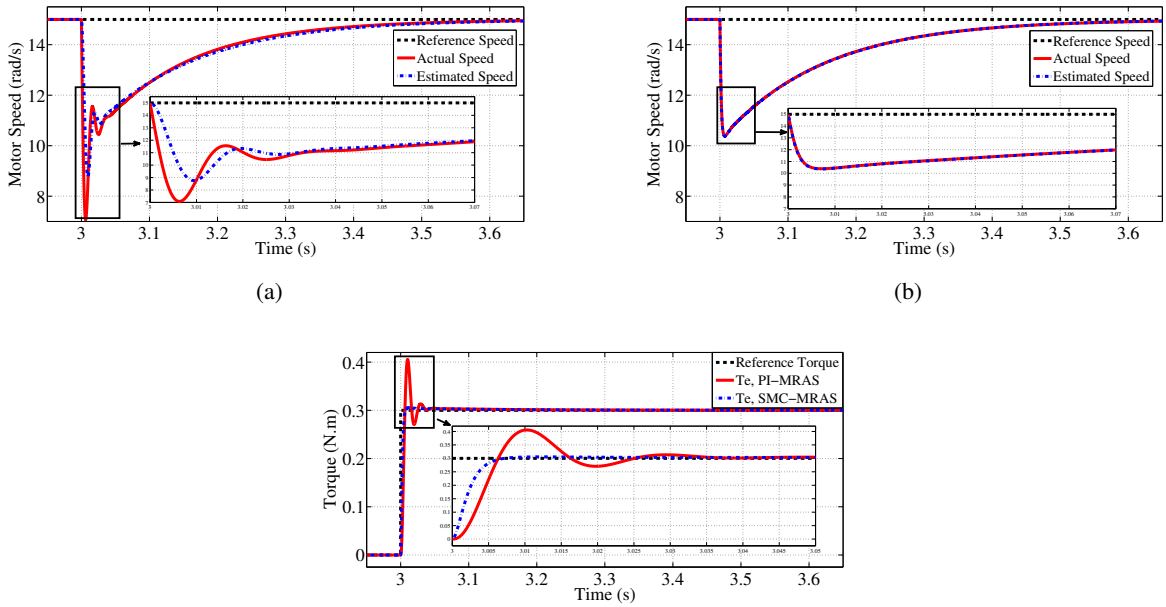

Figure 6. Speed estimator performance of load disturbance rejection capability at 60% rated load. 6(a) PI-MRAS response. 6(b) SMC-MRAS response 6(c) Motor torque T_e response.

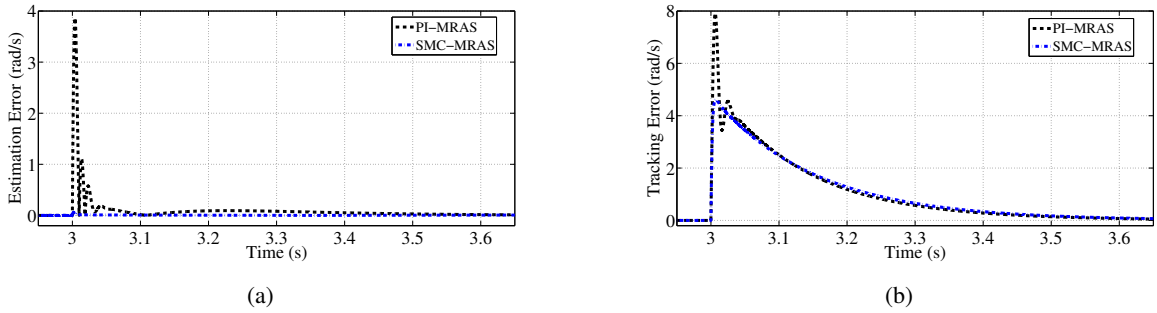

Figure 7. Absolute error of speed. 7(a) estimation error. 7(b) tracking error.

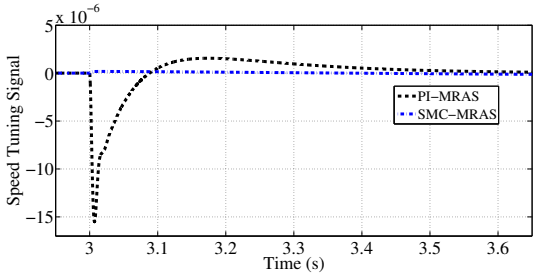

Figure 8. Error signal at 60% rated load.

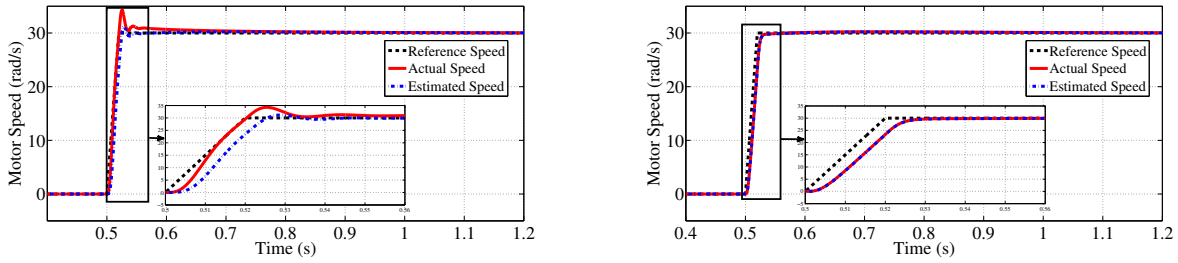

Figure 9. Speed estimator performance during quick acceleration. 9(a) PI-MRAS response. 9(b) SMC-MRAS response.

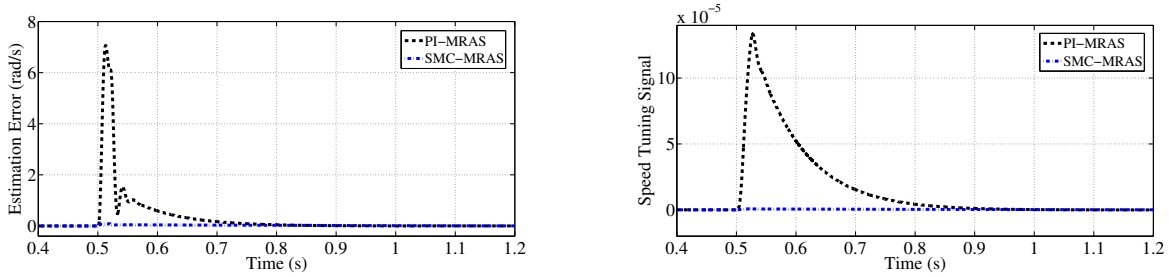

Figure 10. Estimation error and speed error signal.

speed is less deviated. In the proposed SMC-MRAS, the estimation error is reduced from 11.68% to 1.02%. However, the value of the error signal settling time is reduced from $t = 0.941s$ to $t = 0.6s$. These performance parameters are shown in Figures 9 and 10.

6.3. Speed transition from one level to another level at particular load disturbance condition

This simulation case is used to assess the performance of the observer when there is a transition in speed from one level to another. To achieve this, a speed change is made from 40 rad/sec to 10 rad/sec with 60% rated load at time $t = 3s$.

In the recommended speed observer, the estimation error is reduced from 6.52% to 0.88%, and the tracking error is reduced from 19.8% to 11.57%. However, the value of speed tuning signal settling time is reduced from $t = 3.74s$ to $t = 3.19s$. The proposed observer provides an improved speed regulation with minimum tracking and speed estimation errors, as shown in Figures 11 and 12. Additionally, the proposed observer achieves faster convergence of the speed error signal, as shown in Figure 13. However, Figure 14 shows the response of the speed estimator at a 60 rad/sec staircase speed profile.

7. Experimental results & discussion

The practical implementation of the suggested SMC-MRAS was carried out using a DSP-based electric-drive system. Various tests were performed so as to understand the effectiveness of the

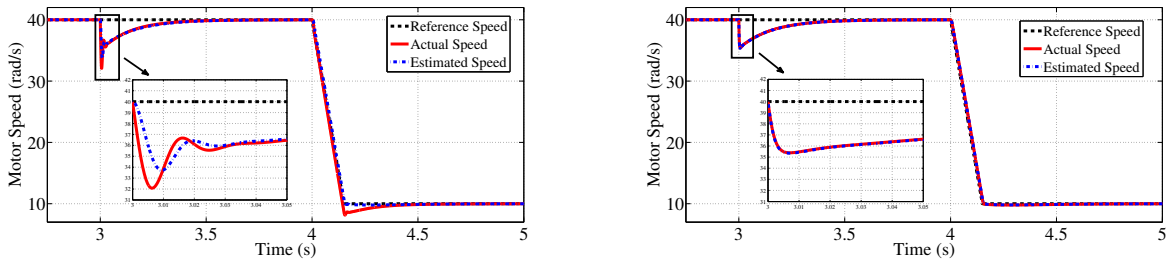

Figure 11. Performance in speed transition. 11(a) PI-MRAS response. 11(b) SMC-MRAS response.

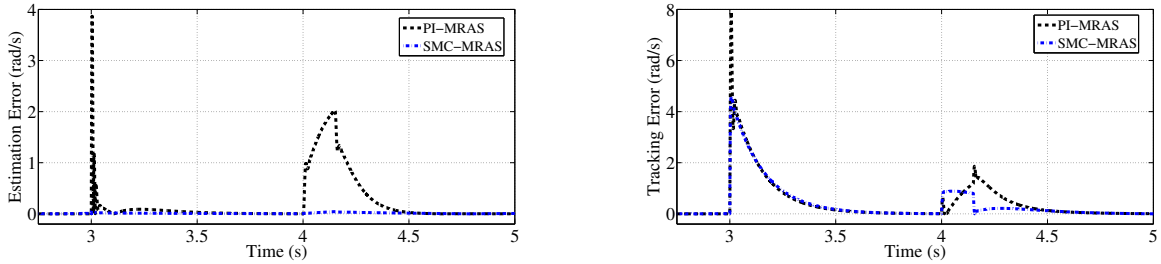

Figure 12. Absolute error of speed. 12(a) Estimation error. 12(b) Tracking error.

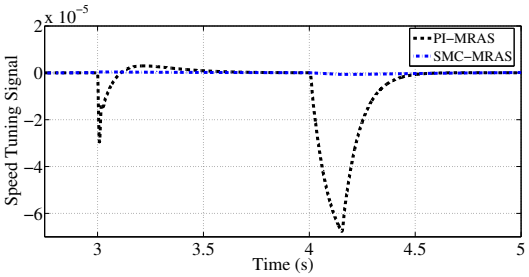

Figure 13. Speed tuning signal.

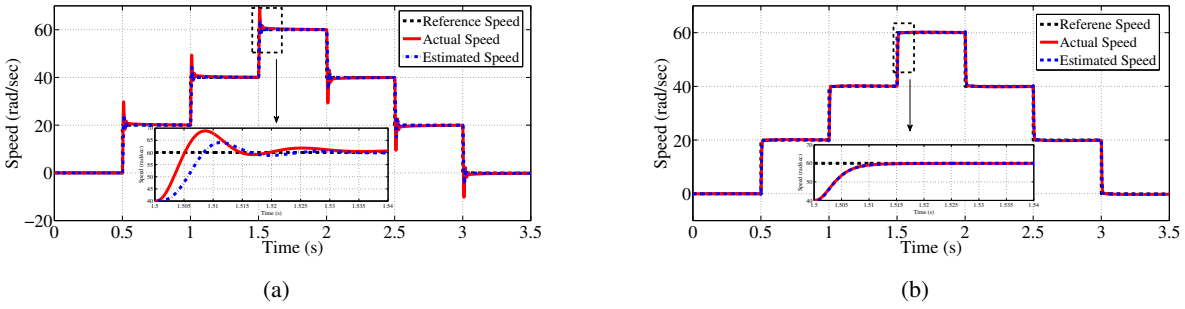

Figure 14. Speed estimator performance at 60 rad/sec staircase. 14(a) PI-MRAS response 14(b) SMC-MRAS response.

newly proposed observer. Throughout these tests, the same PI controller settings were adopted in the induction motor drive system. A 200W four-pole induction motor was utilized for the experiments, and its parameters and specifications can be found in Appendix Table 2. The experimental system is depicted in the schematic diagram presented in Figure 15, while Figure 16 provides a visualization of the real-time setup's implementation.

A 42V DC converter board and the dSPACE DS1104 were employed in the electric drive system. Matlab-Simulink was utilized to implement the proposed scheme in the practical hardware setup. A motor coupling unit was utilized to couple two electric machines. One motor is under test and the second motor provides the load torque profile for the motor under test. However, the converter board used is able to provide two independent, three phase PWM voltages from a constant DC source. The Power electronic board has a complete digital / analog interface with dSPACE board.

For effective implementation of the SMC-MRAS scheme, a high-pass filter is used in order to eliminate integrator drift related issues. The chosen filter corner frequency should be kept as minimal as possible to eliminate any potential DC components. Consequently, a frequency of 1.5 Hz was selected for this purpose. Additionally, in the SMC-MRAS approach, the hitting gain was assigned a value of 0.1. The IM actual speed is measured through the 5,000 pulses/revolution incremental optical encoder. The power electronic inverter was operated at the switching frequency of 15 kHz with a dead time period of $1.5\mu s$.

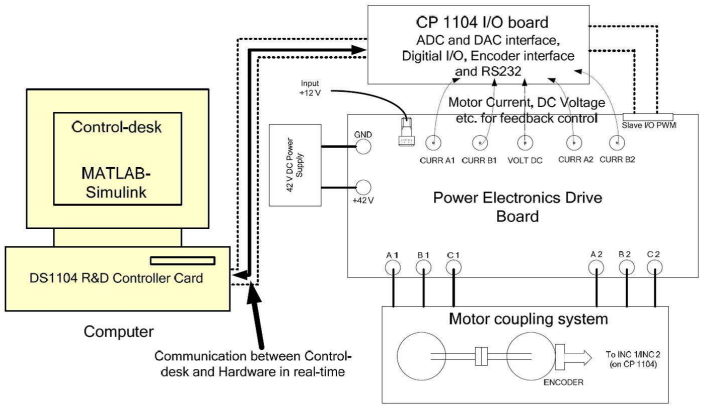

Figure 15. Schematic diagram of experimental system.

7.1. Observer performance at ramp speed profile or during the acceleration mode

In the PI-MRAS analysis, the initial examination involves assessing the speed regulation response of the observer. This assessment employs a ramp reference speed of 60 rad/sec along with a load torque that changes over time. In this specific evaluation, a reference speed of 60 rad/sec is employed to understand the observer's performance under a time varying load between $t = 4s$ and $t = 9s$. The performance of the PI observer is depicted in Figures 17(a) and 17(c), displaying the speed regulation at 60 rad/sec and the applied changing load, respectively. For the SMC-MRAS analysis, a parallel approach is taken, utilizing a comparable speed profile and load torque scenario to appraise the observer's effectiveness. A reference speed of 50 rad/sec is utilized to assess the observer's performance within the time span of $t = 5s$ to $t = 10s$, during which, the applied load torque ranges

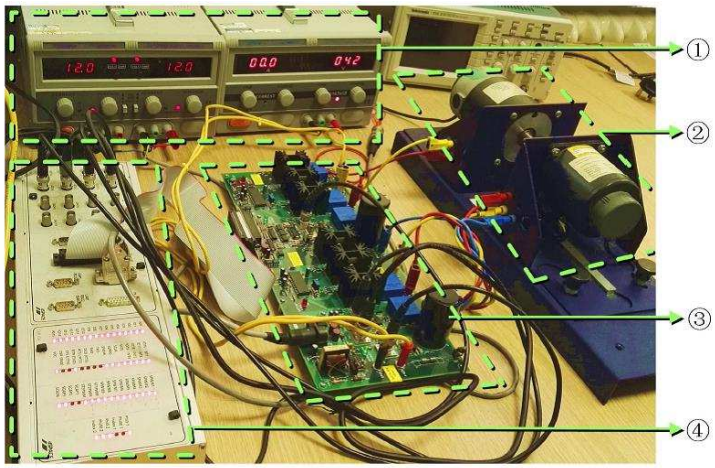

Figure 16. Real time implementation of IM drive experimental system.

from 20% to 70% of the rated load. Figures 17(b) and 17(d) show the speed regulation of the suggested estimator and the applied load, respectively. During the rate of change of velocity or in acceleration mode of operation, the performance of both estimators can be observed in the zoomed Figures 17(e) and 17(f).

The proposed scheme algorithm provides much lower values of both speed estimation and tracking errors, along with the speed regulation performance. The error signal convergence to zero is quicker, which provides an improved error dynamics and transient response. For a better performance understanding, the deviation in response between both estimators at $t = 0.8s$ is zoomed during the acceleration mode of operation. In the case of SMC-MRAS, the estimation error is reduced from 30.25% to 18.12%, and the tracking error is reduced from 58.55% to 26.58%.

7.2. Performance during speed transition and staircase speed profile

This test involves examining how well an observer's speed regulation responds as the motor speed goes from a positive 60 rad/sec to a negative -60 rad/sec. This test covers both forward and reverse motor operations with an applied load variation. During this test, a load equivalent to around 90% of the rated load is used from $t = 1s$ to $t = 15s$. The speed regulation responses of the PI-MRAS for this test, both with the speed transition and the applied load, are depicted in Figures 18(a) and 18(c), respectively. Similarly, the performance of the suggested scheme is displayed in Figures 18(b) SMC-MRAS speed regulation performance, and 18(d) applied load torque during the test. The recommended speed observer provides fast error dynamics with a decreased speed estimation error as compared to PI-MRAS. However, in the case of proposed observer mechanism, the motor speed is less deviated. For a better performance understanding, deviation in response between both estimators at $t = 6.8s$ is zoomed, as shown in Figures 18(e) and 18(f). In the proposed SMC-MRAS, the estimation error is reduced from 48.89% to 26.46%. However, the tracking error is reduced from 74.2% to 54.72%.

Subsequently, the performance of both observers are assessed using a staircase speed profile. The speed regulation response of this staircase profile at 80 rad/sec under a constant load condition

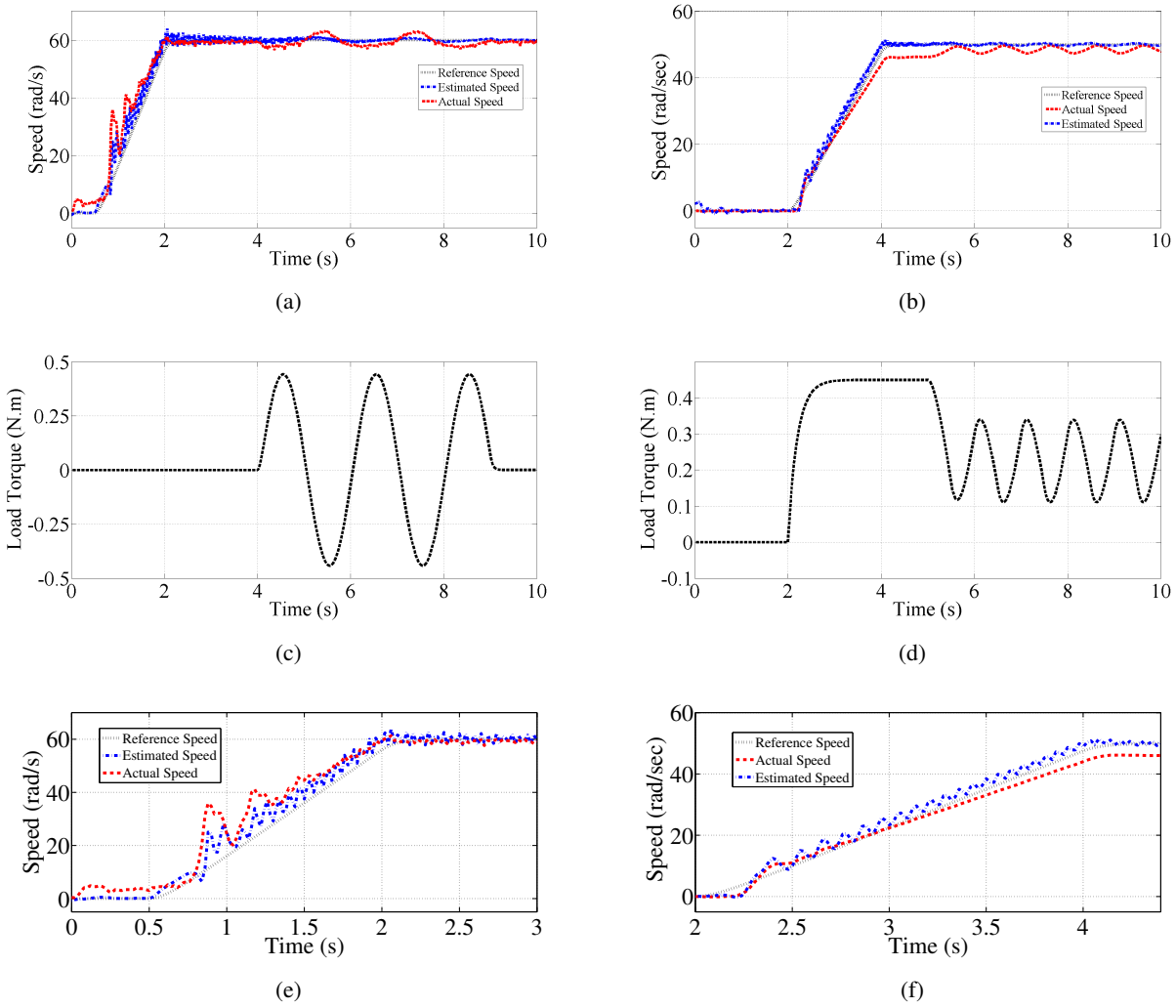

Figure 17. Speed regulation performance of Observer using ramp speed profile with time variant load torque Fig. 17(a) PI-MRAS response Fig. 17(b) SMC-MRAS response Fig.17(c) applied torque PI-MRAS Fig. 17(d) applied torque SMC-MRAS Fig. 17(e) Zoomed of 17(a) Fig. 17(f) Zoomed of 17(b).

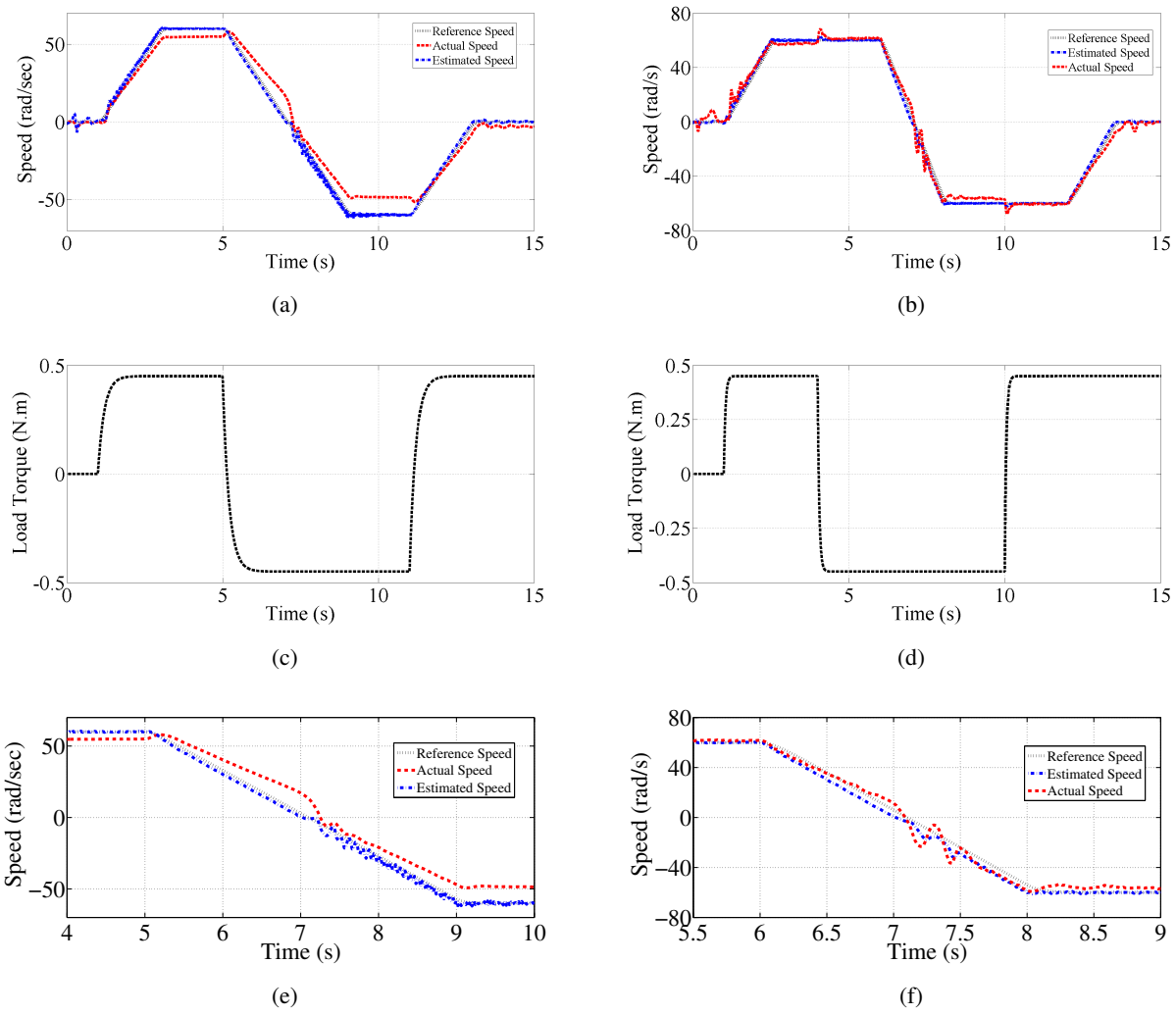

Figure 18. Speed regulation performance of Observer using speed transition profile with time variant load torque Fig. 18(a) PI-MRAS Fig. 18(b) SMC-MRAS Fig. 18(c) applied torque PI-MRAS Fig. 18(d) applied torque SMC-MRAS Fig. 18(e) Zoomed of 18(a) Fig. 18(f) Zoomed of 18(b).

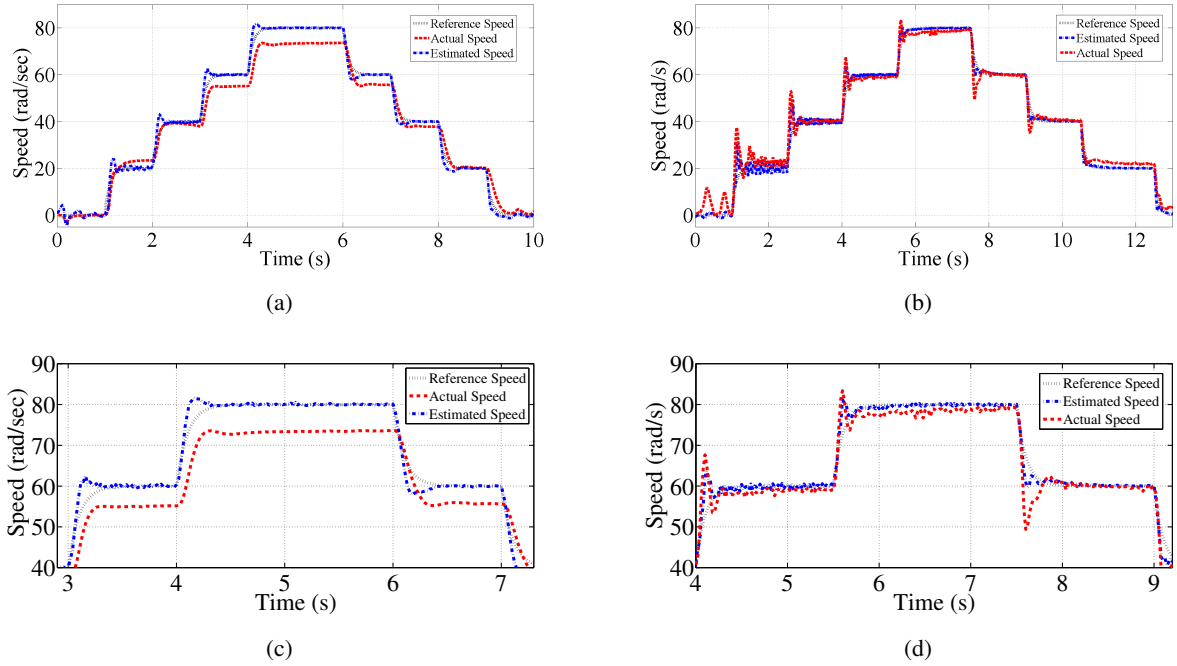

Figure 19. Speed regulation performance of observer using staircase speed profile at 80 rad/sec Fig. 19(a) PI-MRAS response Fig. 19(b) SMC-MRAS response Fig. 19(c) Zoomed of 19(a) Fig. 19(d) Zoomed of 19(b).

is illustrated in Figures 19(a) PI-MRAS, and 19(b) SMC-MRAS. Notably, a more accurate speed estimation is evident when compared to the PI-MRAS method. For the comparison of both estimators, the deviation in response between both estimators at $t = 4.3s$ is zoomed, as shown in Figures 19(c) PI-MRAS, and 19(d) SMC-MRAS. In the recommended speed observer, the estimation error is reduced from 6.19% to 3.8%, and the tracking error is reduced from 11.53% to 8.2%. The proposed observer provides an improved speed regulation with minimal tracking and speed estimation errors, as shown in Figure 19.

8. Conclusions

A new SMC-MRAS speed observer has been presented for sensorless control drive. The Proposed scheme removes the classical MRAS constant gain PI controller with SMC in the adaptation mechanism and utilizes the outer torque error loop for enhanced sensorless drive operation. The stability and dynamics of the proposed scheme were obtained through the Lyapunov theory. For simulation and experimental validation, cases were made according to the vehicle requirements by using different driving speed profiles and load torque. The performance of the SMC-MRAS was evaluated and differentiated with PI-MRAS in the presence of a time variant speed command and load disturbance. Speed regulation, speed tracking and estimation error and convergence of speed tuning signal were considered as key performance indicators. Simulated and experimental results showed that the proposed observer exhibits a good transient response, fast error dynamics and an improved load torque disturbance rejection capability.

Use of AI tools declaration

The authors declare they have not used Artificial Intelligence (AI) tools in the creation of this article.

Conflict of interest

The authors declare that there is no conflicts of interest in this paper.

References

1. Ehsani M, Singh KV, Bansal HO, Mehrjardi RT (2021) State of the Art and Trends in Electric and Hybrid Electric Vehicles. *Proceedings of the IEEE* 109: 967–984. https://doi.org/10.1109/jproc.2021.3072788
2. Sahoo AK, Jena RK (2022) Improved DTC strategy with fuzzy logic controller for induction motor driven electric vehicle. *AIMS Electronics and Electrical Engineering* 6: 296–316. https://doi.org/10.3934/electreng.2022018
3. Liu C, Chau KT, Lee CH, Song Z (2021) A Critical Review of Advanced Electric Machines and Control Strategies for Electric Vehicles. *Proceedings of the IEEE* 109: 1004–1028. https://doi.org/10.1109/jproc.2020.3041417
4. Lee CH, Hua W, Long T, Jiang C, Iyer LV (2021) A Critical Review of Emerging Technologies for Electric and Hybrid Vehicles. *IEEE Open Journal of Vehicular Technology* 2: 471–485. https://doi.org/10.1109/ojvt.2021.3138894
5. De Klerk ML, Saha AK (2021) A Comprehensive Review of Advanced Traction Motor Control Techniques Suitable for Electric Vehicle Applications. *IEEE Access* 9: 125080–125108. https://doi.org/10.1109/access.2021.3110736
6. Shao L, Karci AEH, Tavernini D, Sorniotti A, Cheng M (2020) Design Approaches and Control Strategies for Energy-Efficient Electric Machines for Electric Vehicles—A Review. *IEEE Access* 8: 116900–116913. https://doi.org/10.1109/access.2020.2993235
7. Wang Z, Ching TW, Huang S, Wang H, Xu T (2021) Challenges Faced by Electric Vehicle Motors and Their Solutions. *IEEE Access* 9: 5228–5249. https://doi.org/10.1109/access.2020.3045716
8. Finch JW, Giaouris D (2008) Controlled AC Electrical Drives. *IEEE T Ind Electron* 55: 481–491. https://doi.org/10.1109/tie.2007.911209
9. Jo GJ, Choi JW (2022) Rotor Flux Estimator Design With Offset Extractor for Sensorless-Driven Induction Motors. *IEEE T Power Electron* 37: 4497–4510. https://doi.org/10.1109/tpel.2021.3126331
10. Smith AN, Gadoue SM, Finch JW (2016) Improved Rotor Flux Estimation at Low Speeds for Torque MRAS-Based Sensorless Induction Motor Drives. *IEEE T Energy Conver* 31: 270–282. https://doi.org/10.1109/tec.2015.2480961
11. Gou L, Wang C, Zhou M, You X (2020) Integral Sliding Mode Control for Starting Speed Sensorless Controlled Induction Motor in the Rotating Condition. *IEEE T Power Electron* 35: 4105–4116. https://doi.org/10.1109/tpel.2019.2933599

12. Das S, Kumar R, Pal A (2019) MRAS-Based Speed Estimation of Induction Motor Drive Utilizing Machines d- and q-Circuit Impedances. *IEEE T Ind Electron* 66: 4286–4295. https://doi.org/10.1109/tie.2018.2860530
13. Sun W, Wang Z, Xu D, Wang B (2020) Robust Stability Improvement for Speed Sensorless Induction Motor Drive at Low Speed Range by Virtual Voltage Injection. *IEEE T Ind Electron* 67: 2642–2654. https://doi.org/10.1109/tie.2019.2910039
14. Wang H, Ge X, Liu YC (2018) Second-Order Sliding-Mode MRAS Observer-Based Sensorless Vector Control of Linear Induction Motor Drives for Medium-Low Speed Maglev Applications. *IEEE T Ind Electron* 65: 9938–9952. https://doi.org/10.1109/tie.2018.2818664
15. Reddy CU, Prabhakar KK, Singh AK, Kumar P (2020) Speed Estimation Technique Using Modified Stator Current Error-Based MRAS for Direct Torque Controlled Induction Motor Drives. *IEEE Journal of Emerging and Selected Topics in Power Electronics* 8: 1223–1235. https://doi.org/10.1109/jestpe.2019.2901523
16. Wang H, Yang Y, Chen D, Ge X, Li S, Zuo Y (2022) Speed-Sensorless Control of Induction Motors With an Open-Loop Synchronization Method. *IEEE Journal of Emerging and Selected Topics in Power Electronics* 10: 1963–1977. https://doi.org/10.1109/jestpe.2021.3050805
17. Rind S J, Ren Y, Hu Y, Wang J, Jiang L (2017) Configurations and control of traction motors for electric vehicles: A review. *Chinese Journal of Electrical Engineering* 3: 1–17. https://doi.org/10.23919/cjee.2017.8250419
18. Gadoue SM, Giaouris D, Finch JW (2010) MRAS Sensorless Vector Control of an Induction Motor Using New Sliding-Mode and Fuzzy-Logic Adaptation Mechanisms. *IEEE T Energy Conver* 25: 394–402. https://doi.org/10.1109/tec.2009.2036445
19. Wang T, Wang B, Yu Y, Xu D (2023) Discrete Sliding-Mode-Based MRAS for Speed-Sensorless Induction Motor Drives in the High-Speed Range. *IEEE T Power Electron* 38: 5777–5790. https://doi.org/10.1109/tpel.2023.3236024
20. Nurettin A, İnanç N (2023) Sensorless Vector Control for Induction Motor Drive at Very Low and Zero Speeds Based on an Adaptive-Gain Super-Twisting Sliding Mode Observer. *IEEE Journal of Emerging and Selected Topics in Power Electronics*, 11(4), 4332–4339. https://doi.org/10.1109/jestpe.2023.3265352
21. Zhou M, Cheng S, Feng Y, Xu W, Wang L, Cai W (2022) Full-Order Terminal Sliding-Mode-Based Sensorless Control of Induction Motor With Gain Adaptation. *IEEE Journal of Emerging and Selected Topics in Power Electronics* 10: 1978–1991. https://doi.org/10.1109/jestpe.2021.3081863
22. Zuo Y, Lai C, Iyer KLV (2023) A Review of Sliding Mode Observer Based Sensorless Control Methods for PMSM Drive. *IEEE T Power Electron* 38: 11352–11367. https://doi.org/10.1109/tpel.2023.3287828
23. Ehsani M, Gao Y, Emadi A (2017) *Modern Electric, Hybrid Electric, and Fuel Cell Vehicles*. 2 Eds, CRC Press. https://doi.org/10.1201/9781420054002
24. Bose BK (2002) *Modern power electronics and AC drives*. 2 Eds, Prentice hall Upper Saddle River.
25. Vas P (1998) *Sensorless vector and direct torque control*. New York: Oxford University Press.
26. Zbede YB, Gadoue SM, Atkinson DJ (2016) Model Predictive MRAS Estimator for Sensorless Induction Motor Drives. *IEEE T Ind Electron* 63: 3511–3521. https://doi.org/10.1109/tie.2016.2521721

27. Schauder C (1992) Adaptive speed identification for vector control of induction motors without rotational transducers. *IEEE T Ind Appl* 28: 1054–1061. https://doi.org/10.1109/28.158829
28. Landau YD (1979) *Adaptive control: The model reference approach*. New York, United States.
29. Benlaloui I, Drid S, Chrifi-Alaoui L, Ouriagli M (2015) Implementation of a New MRAS Speed Sensorless Vector Control of Induction Machine. *IEEE T Energy Conver* 30: 588–595. https://doi.org/10.1109/tec.2014.2366473
30. Lo JC, Kuo YH (1998) Decoupled fuzzy sliding-mode control. *IEEE T Fuzzy Syst* 6: 426–435. https://doi.org/10.1109/91.705510
31. Comanescu M, Xu L (2006) Sliding-mode MRAS speed estimators for sensorless vector control of induction Machine. *IEEE T Ind Electron* 53: 146–153. https://doi.org/10.1109/tie.2005.862303
32. Shyu KK, Shieh HJ (1996) A new switching surface sliding-mode speed control for induction motor drive systems. *IEEE T Power Electr* 11: 660–667. https://doi.org/10.1109/63.506132

Appendix

Table 1. PI-Controller gain values.

Controller Number	k_p	k_i
PI-1	1	6
PI-2	2	16
PI-3	2	16

Table 2. Induction motor parameters.

Motor Parameters	Values
Stator Resistance (R_s)	0.1607 Ω
Rotor Resistance (R_r)	0.1690 Ω
Stator Self Inductance (L_s)	7.2 mH
Rotor Self Inductance (L_r)	7.22 mH
Magnetizing Inductance (L_m)	6.38 mH
Rotor Inertia (J)	0.000145 kgm^2
No of Poles (P)	4
Rated Power	200 W
Rated Speed	3621 rpm